Correspondence to:
J. G. Williams,
jack.williams@uni-heidelberg.de

The Importance of Monitoring Interval for Rockfall Magnitude-Frequency Estimation

Jack G. Williams[1,2] (ID), **Nick J. Rosser**[1] (ID), **Richard J. Hardy**[1] (ID), and **Matthew J. Brain**[1] (ID)

[1]Institute of Hazard, Risk, and Resilience, Department of Geography, Durham University, Durham, UK, [2]3D Geospatial Data Processing Group, Institute of Geography, Heidelberg University, Heidelberg, Germany

Abstract Rockfalls commonly exhibit power law volume-frequency distributions, where fewer large events are observed relative to more numerous small events. Within most inventories, the smallest rockfalls are the most difficult to detect and so may not be adequately represented. A primary challenge occurs when neighboring events within a single monitoring interval are recorded as one, producing ambiguity in event location, timing, volume, and frequency. Identifying measurement intervals that minimize these uncertainties is therefore essential. To address this, we use an hourly data set comprising 8,987 3-D point clouds of a cliff that experiences frequent rockfalls. Multiple rockfall inventories are derived from this data set using change detections for the same 10-month period, but over different monitoring intervals. The power law describing the probability distribution of rockfall volumes is highly sensitive to monitoring interval. The exponent, β, is stable for intervals >12 hr but increases nonlinearly over progressively short timescales. This change is manifested as an increase in observed rockfall numbers, from 1.4×10^3 (30 day intervals) to 1.4×10^4 (1 hr intervals), and a threefold reduction in mean rockfall volume. When the monitoring interval exceeds 4 hr, the geometry of detected rockfalls becomes increasingly similar to that of blocks defined by rock mass structure. This behavior change reveals a time-dependent component to rockfall occurrence, where smaller rockfalls (identifiable from more frequent monitoring) are more sensitive to progressive deformation of the rock mass. Acquiring complete inventories and attributing discrete controls over rockfall occurrence may therefore only be achievable with high-frequency monitoring, dependent upon local lithology.

Plain Language Summary Rockfall inventories are required to model erosion, such as along coastlines or in mountain landscapes, and hazard from rockfall activity. The frequency distribution of rockfall volumes, commonly termed "magnitude-frequency", is important for this modeling and for our understanding of how rockfalls occur and what drives them. For rockfalls and landslides in general, these distributions typically follow a power law, with relatively few larger rockfalls as compared to more numerous small events. Advances in hardware and algorithms have considerably improved the spatial resolution and precision with which a given rock face can be monitored using LiDAR. This has in turn improved our ability to detect small rockfalls, which in sum contribute significantly to overall volume loss from rock slopes in this setting. The improvement in spatial resolution has, however, considerably outpaced improvements in the temporal resolution of monitoring. If the interval between surveys is greater than the return interval of rockfalls, neighboring rockfalls within a single monitoring interval are recorded as one, producing ambiguity in event, timing, and volume. For the latter, this effect may amount to an order of magnitude variation. Our research aimed to examine the timescales over which rockfalls occur, allowing us to identify suitable monitoring intervals to discretize rockfalls. While conventional monitoring campaigns tend to acquire surveys at monthly intervals or longer, we draw upon a 1 hr resolution data set acquired over 10 months. We find that the interval of monitoring has a considerable impact on the probability distribution of measured rockfall volumes. An order of magnitude increase in rockfall numbers and a threefold decrease in mean rockfall volume are observed over timescales (monitoring intervals) of 1 hr, rather than 30 days. This is represented by a change in the power law exponent of the magnitude-frequency relationship, which increases nonlinearly below timescales of ~12 hr. Interestingly, above ~12 hr, the exponent is stable, suggesting that changes in monitoring interval above this timescale will attain almost identical rockfall inventories. We explain this change in behavior by relating the geometry of rockfalls to the geometry of the blocks from which they are released. The average size of rockfalls identified over timescales below ~4 hr is comparable to the scale of individual discontinuities, indicating that fragmented detachments are more likely to control the increase in small

events. As the timescale of rockfall monitoring increases, detachments become more similar to the rock mass structure, indicating structural control on failure. This behavior change suggests that smaller rockfalls are more sensitive to progressive deformation of the rock mass. This type of analysis is required to constrain the timescales over which this process occurs, which is necessary to understand prior to attributing specific drivers (such as storms) to rockfall occurrence.

1. Introduction

Geomorphic processes that erode landscapes involve a broad range of event sizes, commonly characterized by fitting magnitude-frequency curves to event inventories. For mass movement volumes, these models underpin event return period and erosion estimates used in hazard modeling (Fell et al., 2008; Guzzetti et al., 2003) and are important for identifying controls on both individual events and longer-term rock slope behavior (Dussauge et al., 2003; Hungr et al., 1999). Despite this, inherent ambiguities remain in our knowledge of rockfall volume-frequency relationships derived from repeat monitoring (Abellán et al., 2011; Krautblatter & Dikau, 2007; Lato et al., 2009; Wang & Tonon, 2011), primarily due to two effects: superimposition (overlapping of sequential rockfall scars through time) and coalescence (amalgamation of adjacent rockfall scars) (van Veen et al., 2017; Williams et al., 2018). When monitoring intervals exceed event return periods, or the actual rate of erosion, superimposed or amalgamated rockfalls are recorded as single detachments. As a result, the frequencies of the smallest and largest rockfall volumes may either be underestimated or overestimated, respectively. A consequence is that events that would otherwise be observed as larger individual rockfalls may actually be the sum of multiple smaller components (Kromer et al., 2017; Royán et al., 2015; Stock et al., 2012). This is important because the smallest events are often the most numerous, which holds implications for the assessment of both the largest credible and most probable event based upon previous observations (Corominas et al., 2018). Logically, censoring of the smallest events must increase with monitoring interval (T_{int}) and, importantly, when rockfalls may be related in both space and time (Rosser et al., 2007), exactly how remains unknown.

The difficulty in detecting individual rockfalls, where T_{int} is long relative to the timescale of their occurrence, also affects explanations for rockfall timing. A common assumption is that the frequency of rockfall occurrence equates to the time-averaged number of events between surveys. Many attempts therefore draw upon potential triggering conditions, such as rainfall, over a given monitoring period, rather than those conditions at the precise moment of detachment (e.g. Lim et al., 2010). Importantly, however, T_{int} is considerably longer in most studies (e.g., weeks to months) than the timescales over which potential triggers fluctuate (D'Amato et al., 2016) and over which successive rockfall releases can occur from the same location. As a result, it remains difficult to attribute individual rockfall events to discrete triggers due to ambiguities within our measurements of both rockfall volume and timing (e.g., Dietze, Mohadjer, et al., 2017; Dietze, Turowski, et al., 2017; Strunden et al., 2015).

While some studies suggest that these effects are minimal over an entire rockfall inventory, others have shown them to be substantial. For example, less than 1% of rockfalls surveyed with high but variable time resolution (~1 hr) were found to be coincident on the limestone cliffs at Mont Saint-Eynard, France (D'Amato et al., 2016); however, recent work has suggested that aggregation effects can be observed via a rockfall volume-frequency scaling with T_{int}. Comparing ~2- and 15-month intervals, van Veen et al. (2017) showed an increase in the exponent of the power law relationship between rockfall volume and frequency as T_{int} was reduced. The exponent, β, describes the rate of change in the frequency density of different event sizes. The density of rockfall volumes can be modeled by integrating the probability density function, $f(V_R)$:

$$f(V_R) = sV_R^{-\beta} \tag{1}$$

where V_R is the rockfall volume (magnitude), s is the intercept, and β is the exponent (Brunetti et al., 2009). The $f(V_R)$ is evaluated between V_R and $V_R + \delta V$, and an increase in the value of β indicates a rise in the proportion of small events as compared to larger events. This is important in the context of a power law distribution, where small events in sum contribute significantly to overall volume loss. At present, however, no

study has considered the effect of T_{int} over periods sufficient to generate large (>10^4) rockfall inventories in a manner that allows potential censoring to be quantitatively assessed.

An application of terrestrial LiDAR, designed to minimize the effects of rockfall superimposition and coalescence, has been used in this study to measure rockfall volumes from an actively failing coastal rock slope. The objective was to assess changes to the frequency distribution of rockfall volumes over various timescales, derived using a range of monitoring intervals (T_{int}). In doing so, we aimed to explain why T_{int} may hold an influence by relating our findings to the mechanisms of rockfall occurrence and the timescales over which these mechanisms operate.

2. Site Description and Data Collection

Rockfall data are presented from an actively eroding coastal cliff in Whitby, UK. The cliff comprises near-horizontal interbedded Jurassic shales, sandstones, and mudstones, capped with ~2 m of glacial till (Alexander & Gawthorpe, 1993; Rosser et al., 2005). The face is subvertical with dilated jointing and intensive surficial weathering, as exhibited elsewhere along the coastline (de Vilder et al., 2017). Erosion of this stretch of coast (~25 km) is characterized by cliff-averaged retreat rates of 0.059 m a^{-1}, measured between 2014 and 2017. During this period, the maximum observed rockfall volume was 1.5×10^4 m^3 (Benjamin, 2018), although the volume loss is generally dominated by smaller-scale rockfalls with median volumes approaching 1.0×10^{-3} m^3 (Rosser et al., 2013). In this study, rockfalls were identified from terrestrial LiDAR surveys acquired over a 10-month period, between 5 March and 30 December 2015. Eight data gaps occurred as a result of system outages, totaling 73 days of the 301 days monitoring campaign, principally due to failure of the laser scanner between late July and early September. Rockfalls that occurred during these periods are excluded from this analysis.

A total of ~8.9×10^3 surveys were collected at $T_{int} = 1$ hr using our automated rockfall monitoring system, which operates from a permanent installation mounted in front of the cliff (Figure 1). The resulting point clouds cover a 210 m wide section of 55 m high cliff, with a point spacing of ~0.05 m at the minimum instrument-target range (342 m) and ~0.14 m at the distal portion of the cliff (533 m). As each scan was acquired in 8 min and identical in terms of its configuration, the data are considered near-instantaneous and the remeasurement of any point occurs at $T_{int} = 1$ hr. Atmospheric correction of range measurements was undertaken at 3 hr intervals by scanning six highly reflective reference targets at very high resolution (point spacing ~5.0×10^{-4} m), which were modeled by least squares plane fitting. Correction factors of the order of 1×10^{-5} m were then applied to all points in each point cloud based on the offset to the reference plane.

By examining the local point cloud geometry, a method to identify and filter points of high positional uncertainty, specifically those close to topographic edges, was applied. Edges generate uncertainties in laser measurements that are exacerbated by increases in target range and laser incidence angles. These arise from the averaging of multiple range measurements (x dimension, approximately cliff normal) within a single beam footprint; uncertainty in the position (y dimension, approximately cliff parallel; z dimension, elevation) of the feature within the laser beam footprint (Hodge, 2010); and the tendency for scan lines to systematically include or omit linear features when scan line spacing exceeds the length scale of these features. To overcome this, a 3-D edge detection is applied that uses the ratio between (1) the distance of a point to the center of a fixed-radius neighborhood and (2) the number of points within this neighborhood. For points close to an edge, the distance to the center of the neighborhood (1) is higher. Given that point density varies across the point cloud, this distance must be normalized based on the neighborhood point density (2) to allow the use of a single threshold to classify points on edges. As the laser incidence angle to the surface increases, uncertainties in the range measurement also increase, making these points less reliable for change detection. To address this, the radiometric response (the reflected energy-time distribution) of each individual measurement was used to identify and filter high incidence angle surfaces. While nadir surfaces reflect an energy-time distribution identical to the emitted laser pulse, increasing surface inclination distorts the energy-time distribution of the reflected pulse. The ratio of the emitted to the reflected pulse duration can therefore be used to represent laser incidence angle. The sensitivity analyses for threshold selection are described in Williams et al. (2018) and resulted in an edge threshold >25 (-) and radiometric deviation threshold >5×10^{-4} (-). Imposing these thresholds typically resulted in no more
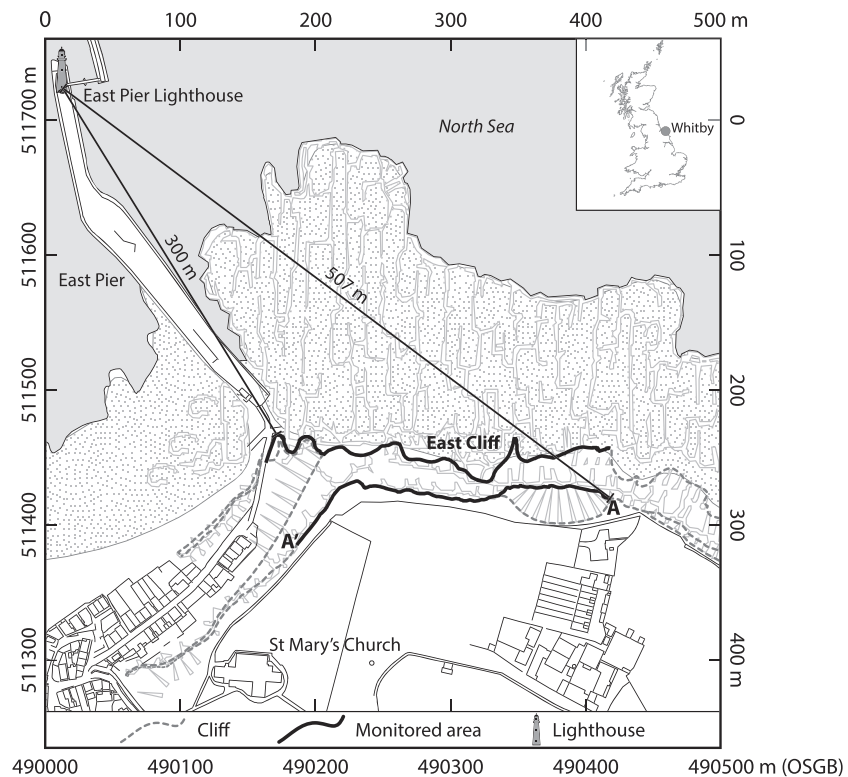
Figure 1. The study site, with the instrument location (East Pier lighthouse) at ~300 m from the monitored cliff face. The system uses a Riegl VZ-1000 terrestrial laser scanner with scan scheduling by SiteMonitor®. Inset shows the position of the site within Great Britain. Transect A-A′ indicates the extent of monitoring along the cliff top, replicated in Figure 2. (Ordnance Survey© Crown Copyright and Database Right 2016. Ordnance Survey, Digimap Licence).

than 15% of the point cloud being removed and reduced the standard deviation of change values between two stable surfaces by 30%.

Change detection was undertaken using a modification of the M3C2 algorithm (Lague et al., 2013) known as DAN VCL. The modification overcomes the considerable uncertainty in change estimates caused by occluded regions within point clouds. When change is calculated along a vector orthogonal to the local surface, the average surface position within each point cloud may vary considerably where there is a paucity of consistently positioned data points. Such regions must be accounted for in near-continuous monitoring, as they are increasingly prevalent within point cloud data captured from a single position (see Williams et al., 2018). Rockfalls were extracted from 2.5-D rasters representing each point cloud and the change relative to the next scan. The resulting rockfall volumes were recorded along with their location, geometry, and timing to within 1 hr. The areal extent of the largest rockfall observed remained an order of magnitude less than the monitored cliff face area. It was therefore unnecessary to impose upper bounds on the resulting rockfall geometries due to monitoring resolution or the extent of the monitored area (Dussauge et al., 2003).

To examine how T_{int} influences the apparent frequency distribution of rockfall volumes, 10 multitemporal inventories were derived from individual surveys separated by increasing values of T_{int} at multihour (1, 3, 6, 12, 24, and 96) and multiday (7, 14, 21, and 30) intervals. Each inventory spanned 270 days. Although shorter than the total 300 days of monitoring, this period provided temporally consistent measurements of surface change with the same start and end date. For the purpose of inventory comparison, the minimum rockfall volume was set by doubling the level of confidence in the change detection from 0.03 to 0.06 m, and the minimum detectable area from 0.15 × 0.15 m (the size of a single pixel) to 0.30 × 0.30 m (supporting information Text S1). While conservative ($V_{min} = 0.0054$ m^3 compared to $V_{min} = 0.0007$ m^3), this approach prevented any instances of noise >0.0007 m^3 from accumulating in proportion to the number of surveys and thereby appearing as numerous small volume events. This ensured that any shift in the frequency density of

recorded erosion volumes was controlled by the interval between surveys (T_{int}), rather than the number of surveys (which increases as T_{int} is lowered).

The exceedance probability of rockfall volumes is provided by the complementary cumulative distribution function (Cirillo, 2013; Clauset et al., 2009):

$$P(V_R) = (V_R \geq V) = \left(\frac{V_R}{V_{min}}\right)^{-\beta - 1} \tag{2}$$

where $P(V_R)$ is the probability of a randomly selected rockfall exceeding a given volume V_R, and the slope is denoted by α (with $\alpha = \beta - 1$; see supporting information Text S2). While the power law may simplify some of the complexities of the inventory (Dussauge et al., 2003), we consider this simplification to be acceptable given that the objective was to compare across multiple distributions. The relationship between T_{int} and β is described using nonlinear least squares estimation, which we used to fit a three-parameter asymptotic function:

$$\beta_{T_{int}} = \beta_0 + C_1 C_2^{\log_{10} T_{int}} \tag{3}$$

where β_0 is the highest value of β when T_{int} is at the finest temporal resolution (here 1 hr). The parameter C_1 is the difference between the value of β when $T_{int} = \infty$ and β_0; and C_2 is a constant that describes the rate of change in β as a function of T_{int}. The parameter C_1 therefore indicates the change in the power law scaling coefficient at the smallest attainable survey interval compared to when $T_{int} \to \infty$, and C_2 describes the timescale over which censoring dominates β as a function of T_{int}. As field observations suggested that rockfalls at this site are never composed of fully disaggregated fine grains of rock, β must tend to a constant at some value of T_{int} below 1 hr.

The underlying controls on rockfall behavior were explored by considering the similarity in rockfall size to that of joint-defined blocks on the cliff face. Block release defined by discontinuities is typically considered to determine individual rockfall geometry (Mavrouli & Corominas, 2017); this is an implicit assumption that underpins how rockfall release is also modeled (e.g., Hoek, 1994). Structure has previously been shown to relate to rockfall size on these cliffs when T_{int} is ~30 days (Barlow et al., 2012; Lim et al., 2010), but examining this control at more frequent monitoring intervals has previously not been possible. A single high-resolution point cloud (~0.02 m point spacing) was therefore collected from three different survey positions after the monitoring period. This was used to generate a full 3-D model of the cliff face with minimal occlusion and, therefore, minimal data gaps. To estimate the size of potential joint-defined rockfall blocks, we extracted aggregated elementary planar objects (*facets*), from the point cloud (visible, exposed, and persistent joint surfaces), considered here to approximate rockfall release surfaces/scars, using the method outlined by Dewez et al. (2016) (see supporting information Text S3). Seven beds exhibited a clearly defined rock mass structure at the cliff face, with the remainder being without clear structure or draped in surficial material. We measured the facets within each of the seven beds to derive summary statistics (distribution, mean, and standard deviation in major axis length, $\overline{a}_F$ and σa_F), which were compared directly to rockfall geometry within the bed. Measurement of these facets could not be undertaken in parallel with rockfall detection due to the occlusion within the point clouds acquired from the fixed monitoring position.

3. Results

More than 1.3×10^4 detachments are reported upon from hourly monitoring, with a minimum, maximum, and mean hourly rate of 0, 39, and 1.5 hr^{-1} (Figure 2) and volumes $0.0054 < V_R < 7.25$ m^3. The maximum rockfall volume observed was 2 orders of magnitude lower than previously reported at this location, reflecting a relatively low erosion period (previously reported maximum V_R along this coastline include 12.73 m^3, Vann Jones et al., 2015; 200.4 m^3, Rosser et al., 2005; 2,614.88 m^3, Lim et al., 2010; 1.5×10^4 m^3, Benjamin, 2018). Rockfalls altered 18.9% of the total monitored cliff face area (1,602 m^2), equating to a yield of 0.17 m^3 day^{-1} or an area- and time-averaged erosion rate of 0.015 m a^{-1}. Measured rockfall area (the areal extent in a 2-D view of each rockfall on the cliff face), scaled with measured V_R, adhered to a power law with coefficient $\gamma = 1.152$, and constant $\alpha = -1.265$ ($r^2 = 0.76$; $p < 0.001$).
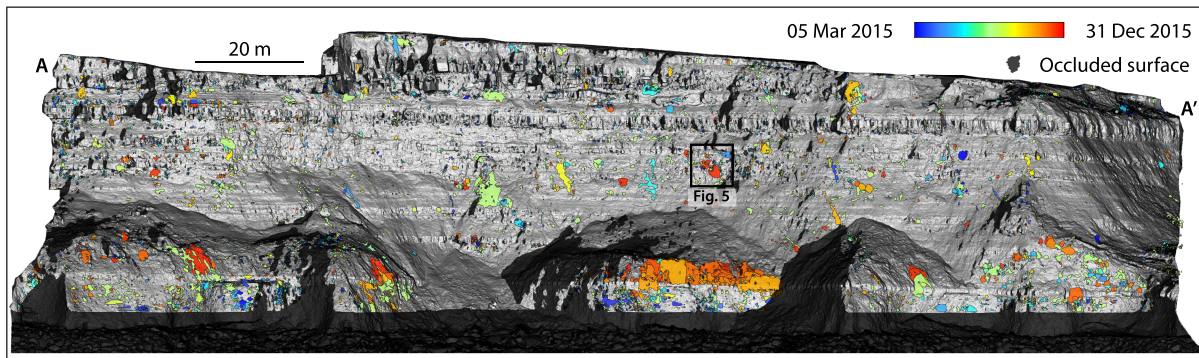
Figure 2. Terrestrial LiDAR-derived surface model of East Cliff Whitby, shown in elevation view. Monitored rockfalls are superimposed and colored by the date and time of occurrence at 1 hr resolution. Transect A-A′ at the cliff top is included for reference in relation to Figure 1. Areal extent of Figure 5 is provided.

Changing T_{int} had a considerable impact on the character of the rockfall inventory. For example, sampling at $T_{int} = 30$ days generated a mean rockfall rate of 6 day^{-1}, whereas $T_{int} = 1$ hr generated 61 day^{-1}; reducing T_{int} from 30 days to 1 hr therefore derived an order of magnitude increase in the total number of observed rockfalls. The mean rockfall volume, $\overline{V_R}$, varies in proportion to T_{int}, whereby $\overline{V_R} = 0.0475$ m^3 when $T_{int} = 30$ days but 0.0169 m^3 when $T_{int} = 1$ hr, equating to a near threefold reduction. The volume-frequency power law coefficient β decreased in an asymptotic manner from $\beta_0 = 2.382$ ($T_{int} = 1$ hr) tending toward $\beta = 1.995$ ($T_{int} = 30$ days), indicating that small rockfalls represent a greater proportion of the total detached material (Figures 3a and 3b; see supporting information Text S3). Fitting equation (3) to the data derived $C_1 = 0.43$ and a rate constant $C_s = 0.09$ ($r^2 = 0.96$, $p < 0.05$). Using out-of-sample estimation to assess the overall model and its predictive capacity, β reached 90% of β_∞ after $T_{int} = 9$ hr, and 99% of β_∞ after $T_{int} = 82$ hr, indicating that β begins to stabilize with increasing T_{int}.

To explore why the volume-frequency relationships vary with T_{int}, we compared rockfall geometry for all monitoring intervals to rock mass structure from beds with visible joint structure. We observe that when T_{int} increased, the difference in mean major axis length between rockfalls and the source rock facets, $\delta\overline{a}$, decreased from positive to negative differences (Figure 4a). The same pattern can be observed in the difference between the standard deviation of major axis lengths for rockfalls and the source rock facets, $\delta\sigma a$. Fitting equation (3), but estimating $\delta\overline{a}$ rather than β as a function of T_{int} (see supporting information Text S7), rock mass structure increasingly controls rockfall block geometry when T_{int} is increased. When plotted using both the mean of $\delta\alpha$ and its range across all beds, rockfalls appear to become more similar to blocks sizes when monitored more frequently. The distributions of rockfall dimensions are shown to become increasingly close to the size distribution of individual facets when T_{int} is reduced (Figure 4b). We note that as facets were measured at 0.02 m resolution as compared to the 0.15 m resolution rockfall data, our observations are not a function of how rockfalls or facets are measured. Their similarity despite this difference in resolution suggests that the rockfall inventory is increasingly dominated by fragments with geometry that is equal to, and possibly smaller than, that of structurally defined blocks/facets.

4. Discussion

4.1. Influence of Monitoring Interval on Observed Rockfalls

Adjusting the interval of rockfall monitoring from 30 days to 1 hr revealed an order of magnitude increase in the apparent number of rockfalls. Given that even the smallest rockfalls can pose a hazard to life (Turner & Jayaprakash, 2012), this increase holds implications for calculations of absolute rockfall hazard in settings where similar behavior may be observed. Where the total sediment yield from rockfalls must remain equal irrespective of T_{int} (cf. Williams et al., 2018), increasing rockfall numbers when $T_{int} \rightarrow 1$ hr must result in smaller rockfalls on average. This behavior is observed here, with a threefold reduction in $\overline{V_R}$ for $T_{int} = 1$ hr, as compared to $T_{int} = 30$ days. Conversely, while our monitoring should not alter the assessment of the largest or worst-case event (Corominas et al., 2017), an increase in $f(V_R)$ and a reduction in $\overline{V_R}$ at the point of release is significant for rockfall remediation (Corominas et al., 2012), for models that predict the
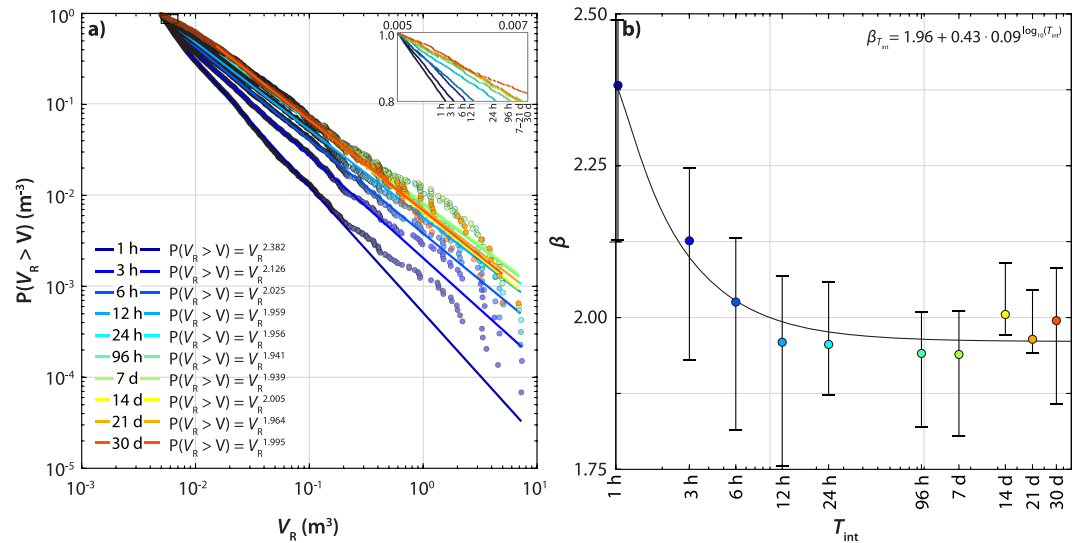
Figure 3. Rockfall magnitude-frequency. (a) Complementary cumulative empirical distributions for rockfalls identified over varying T_{int}, fitted with power laws using the maximum likelihood method (equation (2)). $P(V_R > V)$ represents the probability that a rockfall will exceed volume V. (b) Change in power law scaling exponent β with T_{int}. Solid line shows modeled values of β derived using equation (3). Error bars on β reflect the upper and lower volume estimates for each individual rockfall, which arise based on aerial uncertainty in the scar geometry. Coefficient of determination (r^2) fit to power law, and variation in the decay of β with the LoD applied in rockfall extraction, are provided in supporting information Text S4.

ease with which rockfall debris can be remobilized or weathered based on clast volume or surface area (Messenzehl et al., 2018), and for interpretations of rockfall magnitude-frequency from deposit granulometry (Crosta et al., 2007; Ruiz-Carulla et al., 2017).

Small events both precede and relate to larger events, with the range of rockfall volumes and the high frequency of small fragments pointing to the difficulty in defining rockfalls using minimum volume thresholds
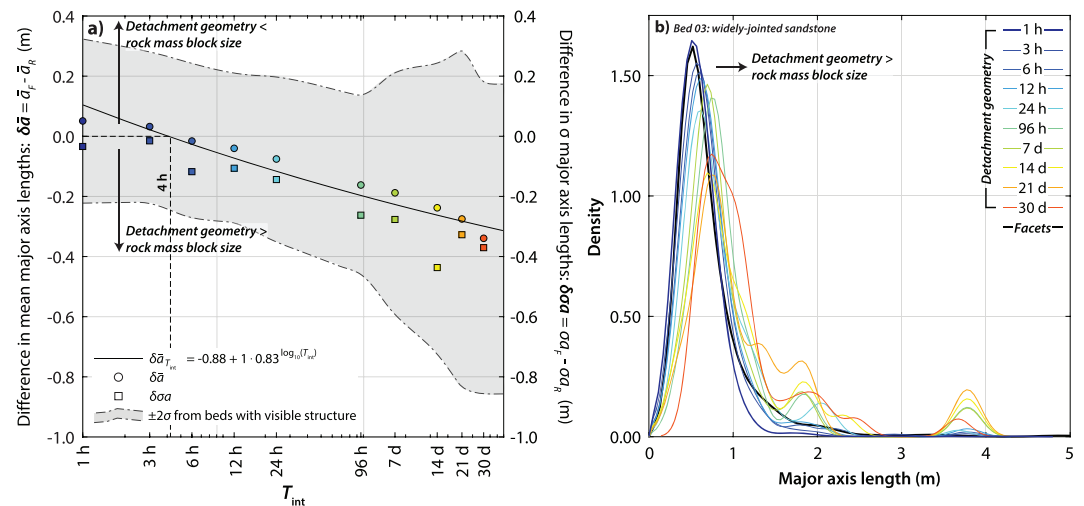

Figure 4. Convergence of rockfall geometry to the geometry of blocks identified in each respective bed, with increasing value of T_{int}. (a) As T_{int} increases, the difference in mean axis lengths between rockfalls and the facets that define the rock mass structure (circles; $\delta\bar{a}$) decreases from ~0, indicating RF sizes match the facet sizes, toward negative values indicating that retrieved RF sizes become larger than those of the facets. This pattern is reflected in the standard deviations of rockfall and facets geometries in each bed (squares). The three-parameter asymptotic regression intersects zero, interpreted as the transition from structural control over rockfall geometry, at $T_{int} = 4$ hr. (b) Distributions of facet major axes lengths and rockfall major axes lengths for a single bed (#3). Distributions for all beds visible in supporting information Text S7.
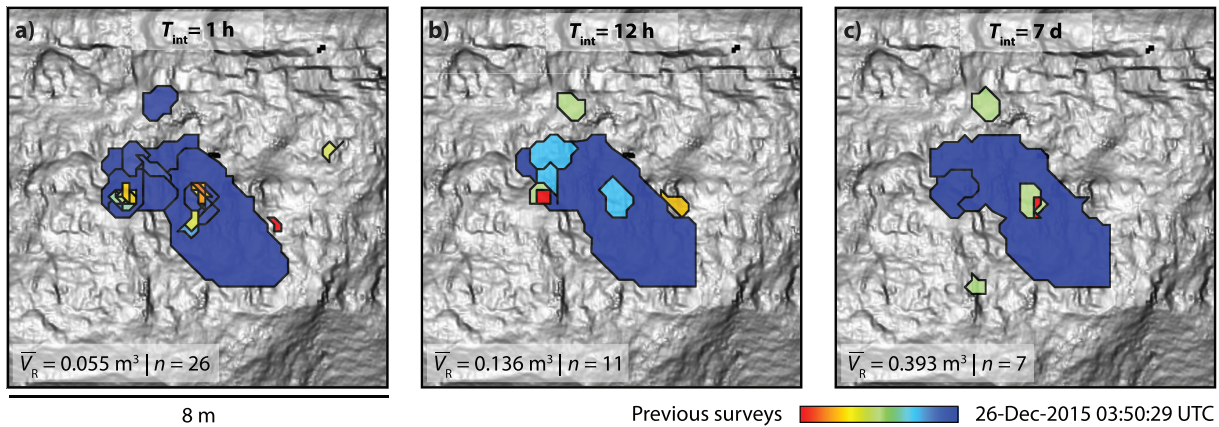
Figure 5. A sequence of rockfalls detected by monitoring at variable T_{int} (1 hr, 12 hr, and 7 days shown) for the area defined in Figure 2. (a) For hourly monitoring, the period presented is 44 days, beginning on 12 November 2015. Prefailure rockfall activity occurs at the upper periphery of the incipient rockfalls. When compared to (b) and (c), a reduction in the number of rockfalls and mean rockfall volume, evident in the change in β with T_{int}, is observed. Variations in rockfall color between plots (a)–(c) emerge because change detections at different surveys intervals are not synchronized.

(cf. Whalley, 1984). Given that only the subvertical regions of cliff were used, we consider all detachments in this study as primary rockfalls released from their original source, as opposed to secondary remobilization of previously failed material (Krautblatter & Dikau, 2007). As we measured individual rockfalls at a point in both time and space when $T_{int} = 1$ hr, we explain the change in volume-frequency scaling at longer intervals as a consequence of larger rockfall events detaching as fragments from within their scar as they fail over time. This is illustrated by the time histories of sequences of fragmented detachments, which occurred within the scars of larger individual rockfalls (e.g., Figure 5). As observed more widely in the probability distribution of rockfall volumes, the impact of reducing T_{int} is both an increase in rockfall numbers and a reduction in $\overline{V_R}$ (Figures 5 and S6). For many rockfalls, fragments are released in a sequence that occurs in response to initial instability, collapse, and then stabilization of the rock face over periods generally shorter than 12 hr (Rosser et al., 2007). This observation highlights the need to consider rockfalls as either (1) individual blocks that could be components of a larger-scale instability, and that are likely to be more prevalent when T_{int} is short or (2) a discrete zone or volume of unstable rock that is released over a period of time via a sequence of related smaller events, and that is likely to be more prevalent in rockfall inventories when T_{int} is long. Our analysis shows that the choice of definition is important and will depend on the application for which the data are acquired. For example, the former definition is applicable in an assessment of absolute hazard or in an assessment of rockfall triggers and mechanisms, where recording the number of individual falling blocks is critical. The latter definition is key for slope stability modeling, which may aim to assess the full extent of a possible area of instability irrespective of failure timing.

4.2. Implications for Rockfall Failure Mechanisms

The increasing proportion of small rockfalls over timescales ≤ 12 hr (Figure 3b), combined with observations of the evolution of individual rockfall scars through time (Figure 5), suggests that rockfall detachment at our site is part of a time-dependent process. The nonlinear relationship between T_{int} and β illustrates that more frequent monitoring captures increasingly small rockfall fragments, but interestingly this is apparent only for intervals where $T_{int} \leq 12$ hr. Specifically, our data provide clear evidence of path dependency between sequential rockfalls, whereby smaller events preferentially occur proximal to, or directly in the location of, other later rockfalls (see supporting information Text S5 and Figure S6). Their occurrence also fits a pattern of increasing frequency and volumes through time, mirroring precursory rockfall behavior observed in lower frequency monitoring (Rosser et al., 2007). If our observations were an artefact of sampling a purely random process in time and space, at reduced values of T_{int}, we would not anticipate such a systematic shift in the volume-frequency scaling. Further, the examined rockfalls are spatially focused, with 18.9% of the total area of rock face having been resurfaced, suggesting that the observed behavior cannot be considered a result of events distributed randomly or extensively across the cliff. This behavior is similar to observations of the incremental release of blocks that combined to form other, larger rockfalls (Kromer et al., 2015; Royán

et al., 2015; Stock et al., 2012). For the first time using a large inventory ($> 10^3$ rockfalls), we put bounds on the timescales over which fragmented detachment operates. In turn, our observations suggest that individual rockfalls could be considered to be (1) part of a process that takes time to evolve via a sequence of block fragments, as a surface expression of an underlying time-dependent mechanism leading to rockfall release (e.g. Rosser et al., 2007); (2) a manifestation of processes that take time to relax back to a quiescent, stable state after failure through an incremental release of fragments as and when kinematically permissible, or via stress redistribution (e.g., Drescher & Handley, 2003; Kimber et al., 1998); (3) occurring in response to the timing, character, and duration of triggering conditions (e.g., storms; D'Amato et al., 2016); or (4) a combination of (1)–(3).

Characterizations of rock masses and rockfalls have conventionally lacked a temporal dimension beyond their probability at a given point in time, where any uncertainty in the latter is often considerably greater than the 1 hr intervals detected here. This temporal dimension enables a description of how rockfalls are likely to respond to discrete triggers, or the timescales of rockfall response to controlling mechanisms described in (1)–(3) above. Similarly, while rockfall inventories describe the duration over which they were compiled, they rarely report a monitoring interval. Where weather conditions, dynamic loading, and time-dependent failure each develop through time and have clear time-dependent effects (e.g., Eppes & Keanini, 2017; Goudie, 2016; Gunzburger et al., 2005), a temporal descriptor of rockfalls and/or rock mass instability that enables comparison between slopes is of value. We propose the use of equation (3) to define the change in volume-frequency scaling as a function of T_{int} and therefore to quantify the widely recognized complexity of how rockfall events evolve and detach (Turner & Jayaprakash, 2012). The approach also enables testing for, and quantification of, the censoring of small events within multitemporal inventories by coalescence and superimposition. The use of the change in volume-frequency power law scaling described offers some advantages in this regard as it is insensitive to individual rockfalls or event rates, providing a means to account for event superimposition and coalescence. An increased understanding of the nature of volume-frequency power law scaling as a function of T_{int} is reliant upon the use of this approach across varying monitoring durations and spatial extents.

4.3. Wider Implications for Understanding Rock Slope Failure

Analysis of the tendency of small rockfalls to approach a geometry defined by the in situ rock mass structure in this setting reveals that here, below $T_{int} = 4$ hr, the discontinuity structure may have a lesser influence on the geometry of the individual fragments that are released. Instead, the geometry of many rockfalls in our inventory appears to be more a function of the time-dependent mass wasting processes than of rock mass strength alone. The smallest detachments we detect may be of a scale that spans both small rockfalls related to discontinuities and rock fracturing, but also detachments associated directly with weathering. Shales and siltstones, for example, undergo surficial weathering creating a frittered crust (Moon & Healy, 1994) that readily releases centimeter-scale platelets (de Vilder et al., 2017).

The timing and location of fragment release observed here implies a failure mechanism that evolves progressively, such as the time-dependent growth of microfractures (Petley et al., 2005) and breakage of rock bridges (Kemeny, 2005). Although here we only capture the spatial and temporal patterns of rockfalls that occur as a consequence of the underlying failure process, our findings concur with forensic studies of rockfall failure mechanisms from these cliffs, whereby a combination of discontinuities and rock bridge breakage are the primary rockfall release mechanisms (de Vilder et al., 2017). Our present study, for the first time, adds clarity around the timing of how and when such rockfalls occur. Where nonpersistent joints are present, the distribution of rock mass damage is strongly related to the presence of rock bridges (Elmo et al., 2018; Guerin et al., 2019; Stead & Eberhardt, 2013). Rockfalls of a size smaller than the discontinuity spacing may not require fracturing through intact rock for release and hence may be more sensitive to external forcing. For rockfalls where release requires the breakage of rock bridges, weakening by weathering or stress redistribution from previous rockfalls is required.

Our inventory comprises rockfalls from across an actively eroding sedimentary coastal cliff; while the rate of mass wasting means that we have been able to collate an inventory consisting of thousands of rockfall events, the variability in release location, and hence lithology, may conflate variations in behavior between individual lithological units. Although it may be reasonable to assume that the disintegration of joint-defined blocks may be a more prevalent process at our coastal sites than in less weathered, or more

massively jointed rock masses, our observations highlight a potentially significant process elsewhere. On more massive and pristine rock masses, the rate constant (C_2) that describes the decay in rockfall volume-frequency scaling with T_{int} may tend to 0. This would indicate that rockfalls occur predominantly via failure of larger, coherent blocks, with little precursory or postfailure fragment loss. In such instances, altering T_{int} would be expected to have a limited influence on β. We note that even in the granodiorite monoliths of Yosemite (California, USA), an incremental pattern of block release over a period of days has been observed when monitoring intervals are short (e.g., Stock et al., 2012). This implies that the behavior described above could be observed with sufficiently high-frequency monitoring even in more massive rock walls; it may therefore capture a time-dependent character that cannot be explained by comparison with structure alone. Identifying settings where this behavior might be observed or is relevant could be based on estimates of β. For example, high values of β, representing a disproportionate contribution of small events to net volume loss, may be likely candidates. Despite this, however, it remains to be demonstrated whether the frequency of small events alone determines if their occurrence is structured in the manner seen here. Examples of settings that might exhibit comparable behavior include weak rocks that are either lithified (e.g., Californian coastal cliffs; Collins & Sitar, 2008), materials where grain size may control the onset of brittle fracturing (e.g., Eberhardt et al., 1999), settings with aggressive weathering (e.g., Krautblatter & Dikau, 2007), or in mining where slopes are cut steep and may be heavily damaged by blasting. In these examples, the effect may be more pronounced, disaggregating the failing mass as it destabilizes over a short time such that large single failures never actually occur (Ruiz-Carulla et al., 2017). In order to better understand the controls on the rate constant C_2, wider testing of equation (3) is required, either using existing data sets where the ratio between monitoring duration and T_{int} is sufficiently high, or through new high-frequency data sets.

4.4. Implications for Rock Slope Monitoring

Our data highlight the importance of selecting a monitoring period, frequency, and extent that is tailored to the aim of the investigation. Notably, it is clear that short interval monitoring is essential to capture the full volume-frequency distribution, wherein the monitoring interval should be chosen with respect to the frequency of the smallest events of interest. Similarly, the duration of the monitoring, or the extent of the area monitored, ideally needs to encompass sufficient numbers of the largest events of interest. Assuming that monitoring frequency is constant, the trade-off between its interval and duration/extent will determine if it is practical to monitor rockfalls in a manner that allows direct links with triggering to be made. Alternatively, our results imply the potential benefits of a sampling strategy with increased monitoring interval, but only when changes are observed in the lead up to a larger rockfall.

If the purpose of monitoring relates to the observation of triggers, it is critical to monitor rockfalls at an interval commensurate with the smallest events of relevance, and a duration that is sufficiently large to sample the largest and least frequent events. The latter is also a function of the monitoring area. For wider rock slope monitoring, one reassurance is that, for timescales of $T_{\text{int}} > 82$ hr in our inventory, β stabilizes to within 1% of its long-term value, β_∞. While defining the equivalent value of T_{int} would be of value for other inventories, these are likely to be consistent and comparable irrespective of the precise monitoring interval used, given that most have $T_{\text{int}} \gg 82$ hr. This observation is of value particularly where large cumulative errors, arising from numerous small but high-frequency events, need to be minimized in long-term monitoring (Williams et al., 2018). Depending on the purpose of the rockfall monitoring, such as to inform erosion modeling, more frequent monitoring may therefore not always be preferable or indeed necessary. For example, in quantifying the long-term retreat of coastal cliffs, volume loss estimates are subject to lower errors when this loss originates from fewer, large events (i.e., from less frequent monitoring) than from sequences of more numerous small events (i.e., from more frequent monitoring over the same period). For hazard estimation from the same cliffs, where arguably even the smallest events captured here could easily be fatal, then there is clear value in high-frequency monitoring. The drawbacks of increased temporal resolution do not extend to the monitoring of all types of surface change. For example, for monitoring across deforming surfaces, such as rock glaciers, a reduction in T_{int} increases the similarity of the surface morphology between surveys, thereby enabling more accurate detection of fine-scale movements (Zahs et al., 2019).

Our study has proposed a method to quantify the timescales of rockfall occurrence, providing a definition for high-frequency monitoring as that which falls beneath the timescale at which β stabilizes. An area where high-frequency monitoring is key is for identifying triggers to mass movements. Where the variability in

triggering conditions operates over minutes to hours, such as rainfall (D'Amato et al., 2016; Krautblatter & Moser, 2009) or thermal effects (Collins & Stock, 2016), rockfall data of a comparable temporal resolution are essential for attributing cause to effect. Without this, relationships will be hindered by the uncertainties that arise from the superimposition and coalescence demonstrated here. The generally low correlation strengths between environmental conditions and rockfall timing presented in several studies (e.g., Rosser et al., 2007; Strunden et al., 2015) are likely to have arisen at least in part due to the temporal averaging of both rockfall and weather data over monthly intervals, or greater. Equally, this may also result from the fact that rockfalls can also be released by smaller perturbations, making the trigger event hard to identify. Given the apparent difficulty in identifying rockfall triggers, some have explored the possibility of lagged effects (e.g., Lim et al., 2010; Strunden et al., 2015). Our findings suggest that monitoring at higher frequencies has the potential both to capture such lagged responses and to observe indicators of the underlying mechanisms, such as small-scale precursory rockfalls, prefailure deformation, or fracture dilation (Carlà et al., 2016; D'Amato et al., 2016; Rosser et al., 2007; Royán et al., 2015). While broad seasonal rockfall patterns or the rockfall response to distinct events can be obvious, even in low-frequency monitoring data, without data captured at a high temporal resolution it will remain difficult to distil a mechanically meaningful understanding of rockfall triggers from time-averaged data alone.

5. Conclusions

High-frequency monitoring over a 10-month period has revealed new insights into the nature of rockfall activity on a coastal cliff. We have identified a high degree of sensitivity of rockfall volume-frequency scaling (magnitude-frequency) to the time between monitoring surveys. When monitoring at long intervals, here $\geq$ 12 hr, the probability distribution of measured rockfall volumes remains ostensibly constant. Below this interval, however, an increasingly short survey interval results in a nonlinear increase in the number of individual rockfalls observed, which on average each have a lower volume than rockfalls observed over longer intervals. Our data suggest that we are observing the separation through time of otherwise superimposed and/or coalesced rockfalls as individual fragments. Our comparison of rockfall geometry to the rock mass structure reveals that predicting individual block size based upon rock mass structure alone may be problematic over short (instantaneous) timescales. Over the longer term, and as monitoring intervals increase, rockfall geometry has been shown to converge with that defined by rock mass structure. Importantly, the data imply that small rockfalls cannot be considered independent in space or time, with the patterns we reveal being indicative of progressive failure mechanisms driving rockfalls that fundamentally display a time dependency. If this behavior is not considered, identifying rockfall triggers and accurately constraining the hazard they pose will remain difficult, due to the underestimation of rockfall frequency and averaging of relationships with external drivers over timescales beyond those of individual rockfall occurrence. With wider use of the relation between monitoring interval and magnitude-frequency exponent (equation (3)), an appraisal of the role of small, frequent events in driving larger events will improve our understanding of the time dependence and drivers of landscape evolution.

References

Abellán, A., Vilaplana, J. M., Calvet, J., García-Sellés, D., & Asensio, E. (2011). Rockfall monitoring by Terrestrial Laser Scanning—Case study of the basaltic rock face at Castellfollit de la Roca (Catalonia, Spain). *Natural Hazards and Earth System Sciences*, *11*, 829–841. https://doi.org/10.5194/nhess-11-829-2011

Alexander, J., & Gawthorpe, R. L. (1993). *The complex nature of a Jurassic multistorey, alluvial sandstone body, Whitby, North Yorkshire*, *Special Publications* (Vol. 73(1), pp. 123–142). London: Geological Society. https://doi.org/10.1144/GSL.SP.1993.073.01.08

Barlow, J., Lim, M., Rosser, N. J., Petley, D. N., Brain, M. J., Norman, E. C., & Geer, M. (2012). Modeling cliff erosion using negative power law scaling of rockfall. *Geomorphology*, *139*, 416–424. https://doi.org/10.1016/j.geomorph.2011.11.006

Benjamin, J. (2018). *Regional-scale controls on rockfall occurrence* (Doctoral dissertation) (Chap. 3). In *Retrieved from [Durham e-theses online]*. Durham: University.

Brunetti, M. T., Guzzetti, F., & Rossi, M. (2009). Probability distributions of landslide volumes. *Nonlinear Processes in Geophysics*, *16*(2), 179–188. https://doi.org/10.5194/npg-16-179-2009

Carlà, T., Intrieri, E., Di Traglia, F., & Casagli, N. (2016). A statistical-based approach for determining the intensity of unrest phases at Stromboli volcano (Southern Italy) using one-step-ahead forecasts of displacement time series. *Natural Hazards*, *84*(1), 669–683. https://doi.org/10.1007/s11069-016-2451-5

Cirillo, P. (2013). Are your data really Pareto distributed? *Physica A*, *392*, 5947–5962. https://doi.org/10.1016/j.physa.2013.07.061

Clauset, A., Shalizi, C. R., & Newman, M. E. J. (2009). Power law distributions in empirical data. *SIAM Review*, *51*(4), 661–703. https://doi.org/10.1137/070710111

Collins, B. D., & Sitar, N. (2008). Processes of coastal bluff erosion in weakly lithified sands, Pacifica, California, USA. *Geomorphology*, *97*, 483–501. https://doi.org/10.1016/j.geomorph.2007.09.004

Collins, B. D., & Stock, G. M. (2016). Rockfall triggering by cyclic thermal stressing of exfoliation fractures. *Nature Geoscience*, *9*, 395–400. https://doi.org/10.1038/ngeo2686

Corominas, J., Mavrouli, O., & Ruiz-Carulla, R. (2017). Rockfall Occurrence and Fragmentation. In K. Sassa, M. Mikoš, & Y. Yin (Eds.), *Advancing culture of living with landslides. Workshop on World Landslide Forum 2017* (pp. 75–97). Cham: Springer. https://doi.org/10.1007/978-3-319-59469-9_4

Corominas, J., Mavrouli, O., & Ruiz-Carulla, R. (2018). Magnitude and frequency relations: are there geological constraints to the rockfall size? *Landslides*, *15*(5), 829–845. https://doi.org/10.1007/s10346-017-0910-z

Corominas, J., Mavrouli, O., Santana, D., & Moya, J. (2012). Simplified approach for obtaining the block volume distribution of fragmental rockfall. In E. Eberhardt, C. Frose, K. Turner, & S. Leroueil (Eds.), *Proceedings of the 11th International Symposium on Landslides, Banff, Canada* (Vol. 2, pp. 1159–1164). CRC Press: Balkema.

Crosta, G. B., Frattini, P., & Fusi, N. (2007). Fragmentation in the Val Pola rock avalanche, Italian Alps. *Journal of Geophysical Research, Earth Surface*, *112*(F1). https://doi.org/10.1029/2005JF000455

D'Amato, J., Hantz, D., Guerin, A., Jaboyedoff, M., Baillet, L., & Mariscal, A. (2016). Influence of meteorological factors on rockfall occurrence in a middle mountain limestone cliff. *Natural Hazards and Earth System Sciences*, *16*, 719–735. https://doi.org/10.5194/nhess-16-719-2016

de Vilder, S. J., Rosser, N. J., & Brain, M. J. (2017). Forensic analysis of rockfall scars. *Geomorphology*, *295*, 202–214. https://doi.org/10.1016/j.geomorph.2017.07.005

Dewez, T. J. B., Girardeau-Montaut, D., Allanic, C., & Rohmer, J. (2016). FACETS: A CloudCompare plugin to extract geological planes from unstructured 3D point clouds. *International Archives of the Photogrammetry, Remote Sensing and Spatial Information Sciences*, *XLI-B5*, 799–804. https://doi.org/10.5194/isprs-archives-XLI-B5-799-2016

Dietze, M., Mohadjer, S., Turowski, J. M., Ehlers, T. A., & Hovius, N. (2017). Seismic monitoring of small alpine rockfalls–validity, precision and limitations. *Earth Surface Dynamics*, *5*(4), 653–668. https://doi.org/10.5194/esurf-5-653-2017

Dietze, M., Turowski, J. M., Cook, K. L., & Hovius, N. (2017). Spatiotemporal patterns, triggers and anatomies of seismically detected rockfalls. *Earth Surface Dynamics*, *5*, 757–779. https://doi.org/10.5194/esurf-5-757-2017

Drescher, K., & Handley, M. F. (2003). Aspects of time-dependent deformation in hard rock at great depth. *Journal of the South African Institute of Mining and Metallurgy*, *103*(5), 325–335.

Dussauge, C., Grasso, J., & Helmstetter, A. (2003). Statistical analysis of rockfall volume distributions: Implications for rockfall dynamics. *Journal of Geophysical Research*, *108*(B6), 2286–2307. https://doi.org/10.1029/2001JB000650

Eberhardt, E., Stimpson, B., & Stead, D. (1999). Effects of grain size on the initiation and propagation thresholds of stress-induced brittle fractures. *Rock Mechanics and Rock Engineering*, *32*(2), 81–89. https://doi.org/10.1007/s006030050026

Elmo, D., Donati, D., & Stead, D. (2018). Challenges in the characterisation of intact rock bridges in rock slopes. *Engineering Geology*, *245*, 81–96. https://doi.org/10.1016/j.enggeo.2018.06.014

Eppes, M.-C., & Keanini, R. (2017). Mechanical weathering and rock erosion by climate-dependent subcritical cracking. *Reviews in Geophysics*, *55*, 470–508. https://doi.org/10.1002/2017RG000557

Fell, R., Corominas, J., Bonnard, C., Cascini, L., Leroi, E., & Savage, W. Z. (2008). Guidelines for landslide susceptibility, hazard and risk zoning for land-use planning. *Engineering Geology*, *102*(3), 99–111. https://doi.org/10.1016/j.enggeo.2008.03.014

Goudie, A. S. (2016). Quantification of rock control in geomorphology. *Earth-Science Reviews*, *159*, 374–387. https://doi.org/10.1016/j.earscirev.2016.06.012

Guerin, A., Jaboyedoff, M., Collins, B. D., Derron, M. H., Stock, G. M., Matasci, B., et al. (2019). Detection of rock bridges by infrared thermal imaging and modeling. *Scientific Reports*, *9*(1), 1–19. https://doi.org/10.1038/s41598-019-49336-1

Gunzburger, Y., Merrien-Soukatchoff, V., & Guglielmi, Y. (2005). Influence of daily surface temperature fluctuations on rock slope stability: Case study of the Rocher de Valabres slope (France). *International Journal of Rock Mechanics and Mining Sciences*, *42*, 331–349. https://doi.org/10.1016/j.ijrmms.2004.11.003

Guzzetti, F., Reichenbach, P., & Wieczorek, G. F. (2003). Rockfall hazard and risk assessment in the Yosemite Valley, California, USA. *Natural Hazards and Earth System Sciences*, *3*(6), 491–503. https://doi.org/10.5194/nhess-3-491-2003

Hodge, R. A. (2010). Using simulated terrestrial laser scanning to analyse errors in high resolution scan data of irregular surfaces. *ISPRS Journal of Photogrammetry and Remote Sensing*, *65*(2), 227–240. https://doi.org/10.1016/j.isprsjprs.2010.01.001

Hoek, E. (1994). Strength of rock masses. *ISRM News*, *2*, 4–16.

Hungr, O., Evans, S. G., & Hazzard, J. (1999). Magnitude and frequency of rock falls and rock slides along the main transportation corridors of southwestern British Columbia. *Canadian Geotechnical Journal*, *36*, 224–238. https://doi.org/10.1139/t98-106

Kemeny, J. (2005). Time-dependent drift degradation due to the progressive failure of rock bridges along discontinuities. *International Journal of Rock Mechanics and Mining Sciences*, *42*(1), 35–46. https://doi.org/10.1016/j.ijrmms.2004.07.001

Kimber, O. G., Allison, R. J., & Cox, N. J. (1998). Mechanisms of failure and slope development in rock masses. *Transactions of the Institute of British Geographers*, *23*, 353–370. https://doi.org/10.1111/j.0020-2754.1998.00353.x

Krautblatter, M., & Dikau, R. (2007). Towards a uniform concept for the comparison and extrapolation of rockwall retreat and rockfall supply. *Geografiska Annaler. Series A, Physical Geography*, *89*, 21–40. https://doi.org/10.1111/j.1468-0459.2007.00305.x

Krautblatter, M., & Moser, M. (2009). A nonlinear model coupling rockfall and rainfall intensity based on a four-year measurement in a high Alpine rock wall (Reintal, German Alps). *Natural Hazards and Earth System Sciences*, *9*(4), 1425–1432. https://doi.org/10.5194/nhess-9-1425-2009

Kromer, R. A., Hutchinson, D. J., Lato, M. J., Gauthier, D., & Edwards, T. (2015). Identifying rock slope failure precursors using LiDAR for transportation corridor hazard management. *Engineering Geology*, *195*, 93–103. https://doi.org/10.1016/j.enggeo.2015.05.012

Kromer, R. A., Lato, M. J., Hutchinson, D. J., Gauthier, D., & Edwards, T. (2017). Managing rockfall risk through baseline monitoring of precursors using a terrestrial laser scanner. *Canadian Geotechnical Journal*, *54*(7), 953–967. https://doi.org/10.1139/cgj-2016-0178

Lague, D., Brodu, N., & Leroux, J. (2013). Accurate 3D comparison of complex topography with terrestrial laser scanner: Application Rangitikei canyon (NZ). *ISPRS Journal of Photogrammetry and Remote Sensing*, *82*, 10–26. https://doi.org/10.1016/j.isprsjprs.2013.04.009

Lato, M. J., Hutchinson, D. J., Diederichs, M., Ball, D., & Harrap, R. (2009). Engineering monitoring of rockfall hazards along transportation corridors: using mobile terrestrial LiDAR. *Natural Hazards and Earth System Sciences*, *9*, 935–946. https://doi.org/10.5194/nhess-9-935-2009

Lim, M., Rosser, N. J., Allison, R., & Petley, D. N. (2010). Erosional processes in the hard rock coastal cliffs at Staithes, North Yorkshire. *Geomorphology*, *114*, 12–21. https://doi.org/10.1016/j.geomorph.2009.02.011

Mavrouli, O., & Corominas, J. (2017). Comparing rockfall scar volumes and kinematically detachable rock masses. *Engineering Geology*, *219*, 63–74. https://doi.org/10.1016/j.enggeo.2016.08.013

Messenzehl, K., Viles, H., Otto, J.-C., Ewald, A., & Dikau, R. (2018). Linking rock weathering, rockwall instability and rockfall supply on talus slopes in glaciated hanging valleys (Swiss Alps). *Permafrost and Periglacial Processes*, *29*, 135–151. https://doi.org/10.1002/ppp.1976

Moon, V. G., & Healy, T. (1994). Mechanisms of coastal cliff retreat and hazard zone delineation in soft flysch deposits. *Journal of Coastal Research*, *10*(3), 663–680.

Petley, D. N., Higuchi, T., Petley, D. J., Bulmer, M. H., & Carey, J. (2005). Development of progressive landslide failure in cohesive materials. *Geology*, *33*(3), 201–204. https://doi.org/10.1130/G21147.1

Rosser, N. J., Brain, M. J., Petley, D. N., Lim, M., & Norman, E. C. (2013). Coastline retreat via progressive failure of rocky coastal cliffs. *Geology*, *41*(8), 939–942. https://doi.org/10.1130/G34371.1

Rosser, N. J., Lim, M., Petley, D. N., Dunning, S. A., & Allison, R. (2007). Patterns of precursory rockfall prior to slope failure. *Journal of Geophysical Research, Earth Surface*, *112*(F4). https://doi.org/10.1029/2006JF000642

Rosser, N. J., Petley, D. N., Lim, M., Dunning, S. A., & Allison, R. J. (2005). Terrestrial laser scanning for monitoring the process of hard rock coastal cliff erosion. *Quarterly Journal of Engineering Geology and Hydrogeology*, *38*, 363–375. https://doi.org/10.1144/1470-9236/05-008

Royán, M. J., Abellán, A., & Vilaplana, J. M. (2015). Progressive failure leading to the 3 December 2013 rockfall at Puigcercós scarp (Catalonia, Spain). *Landslides*, *12*(3), 585–595. https://doi.org/10.1007/s10346-015-0573-6

Ruiz-Carulla, R., Corominas, J., & Mavrouli, O. (2017). A fractal fragmentation model for rockfalls. *Landslides*, *14*(3), 875–889. https://doi.org/10.1007/s10346-016-0773-8

Stead, D., & Eberhardt, E. (2013). Understanding the mechanics of large landslides. *Italian Journal of Engineering Geology and Environment Book Series*, *6*, 85–112. https://doi.org/10.4408/IJEGE.2013-06.B-07

Stock, G. M., Martel, S. J., Collins, B. D., & Harp, E. L. (2012). Progressive failure of sheeted rock slopes: The 2009–2010 Rhombus Wall rock falls in Yosemite Valley, California, USA. *Earth Surface Processes and Landforms*, *37*(5), 546–561. https://doi.org/10.1002/esp.3192

Strunden, J., Ehlers, T. A., Brehm, D., & Nettesheim, M. (2015). Spatial and temporal variations in rockfall determined from TLS measurements in a deglaciated valley, Switzerland. *Journal of Geophysical Research, Earth Surface*, *120*(7), 1251–1273. https://doi.org/10.1002/2014JF003274

Turner, A. K., & Jayaprakash, G. P. (2012). Introduction. In A. K. Turner & R. L. Schuster (Eds.), *Rockfall characterization and control* (pp. 3–20). Washington D.C.: Transportation Research Board, National Academy of Sciences.

van Veen, M., Hutchinson, D. J., Bonneau, D. A., Sala, Z., Ondercin, M., & Lato, M. (2017). Combining temporal 3D remote sensing data with spatial rockfall simulations for improved understanding of hazardous slopes within rail corridors. *Natural Hazards and Earth System Sciences*, *18*, 2295–2308. https://doi.org/10.5194/nhess-2017-392

Vann Jones, E. C., Rosser, N. J., Brain, M. J., & Petley, D. N. (2015). Quantifying the environmental controls on erosion of a hard rock cliff. *Marine Geology*, *363*, 230–242. https://doi.org/10.1016/j.margeo.2014.12.008

Wang, Y., & Tonon, F. (2011). Discrete element modeling of rock fragmentation upon impact in rock fall analysis. *Rock Mechanics and Rock Engineering*, *44*, 23–35. https://doi.org/10.1007/s00603-010-0110-9

Whalley, W. B. (1984). Rockfalls. In D. Brunsden & D. B. Prior (Eds.), *Slope instability* (pp. 217–225). New York: Wiley.

Williams, J. G., Rosser, N. J., Hardy, R. J., Brain, M. J., & Afana, A. A. (2018). Optimising 4D approaches to surface change detection: Improving understanding of rockfall magnitude-frequency. *Earth Surface Dynamics*, *6*, 101–119. https://doi.org/10.5194/esurf-6-101-2018

Zahs, V., Hämmerle, M., Anders, K., Hecht, S., Sailer, R., Rutzinger, M., et al. (2019). Multi-temporal 3D point cloud-based geomorphological deformation analysis at an Alpine Rock Glacier using airborne and terrestrial LiDAR. *Permafrost and Periglacial Processes*, *30*, 222–238. https://doi.org/10.1002/ppp.2004